ResearchOnline@JCU



This is the author-created version of the following work:

Kamel, Michael S.A., Stoppiello, Craig Thomas, and Jacob, Mohan V. (2023)

Improved Transfer-Free Sustainable Graphene Electrode using Silver Nanowires
for Organic Photovoltaics. ACS Applied Energy Materials, 6 (21) pp. 1116811178.

Access to this file is available from:

https://researchonline.jcu.edu.au/81427/

© 2023 American Chemical Society.

Please refer to the original source for the final version of this work:

https://doi.org/10.1021/acsaem.3c02001

Improved transfer-free sustainable graphene electrode using silver nanowires for organic photovoltaics

Michael S. A. Kamel^{a, b}, Craig Thomas Stoppiello ^c and Mohan V. Jacob^{*a}

^a Electronic Materials Research Lab, College of Science and Engineering, James Cook University,

Townsville 4811, Australia

^b Physics Department, Faculty of Science, Minia University, P.O. Box 61519 Minia, Egypt

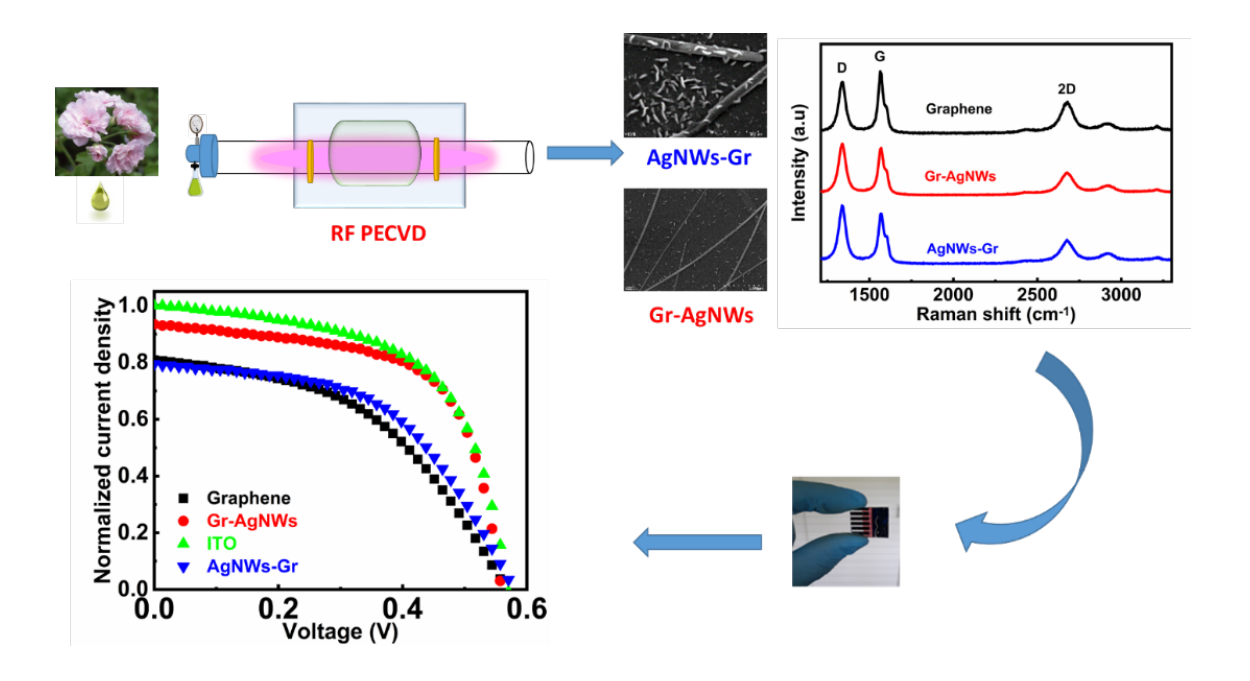
^c Centre for Microscopy and Microanalysis, The University of Queensland, Australia.

Email: mohan.jacob@jcu.edu.com

Abstract

The hybridization of silver nanowires (AgNWs) and chemical vapor deposition (CVD) based graphene is a promising strategy to produce efficient transparent conducting electrodes (TCEs) for organic photovoltaics (OPVs). In this work, we successfully demonstrate the coupling of transfer-free graphene fabricated on glass using plasma enhanced CVD from sustainable carbon source with AgNWs and hence avoided multistep procedure to transfer graphene and damages. The resulting hybrid TCEs exhibit lower sheet resistance compared to the pristine graphene. In addition, the growth of vertically oriented-graphene nanosheets suppress the impact of the rough surface of AgNWs and increases the area of interface between the TCE and the active layer. OPV devices developed on the hybrid TCE, with active layers namely, P3HT: PCBM, P3HT: PC70BM, and PM6: Y6 show a comparable performance of the reference device. For instance, P3HT: PCBM-based device on the hybrid electrode exhibits higher fill factor (0.63) and a comparable power conversion efficiency (2.18%) to that of the ITO-counterpart (0.60 and 2.22%). Similarly, the PM6:Y6-device fabricated on the hybrid TCE demonstrates analogous efficiency (9.75%) to that on ITO (10.3%). The present work demonstrates an auspicious platform towards sustainable and economic production of efficient transfer-free graphenebased TCEs for OPVs.

Graphical Abstract:



Keywords

Transparent conducting electrode; Transfer-free graphene; Silver nanowires; Organic photovoltaics; Fill factor

1. Introduction

Indium tin oxide (ITO) has been widely used as a transparent conductive electrode (TCE) for organic solar cells (OSCs) thanks to its remarkable electrical and optical properties [1-3]. However, the high cost, scarcity of indium, poor chemical and mechanical stabilities of ITO necessitate the development of ITO-free OSCs [4-7]. Several TCE candidates including PEDOT: PSS [8], metal oxides [9], metal thin films [10], and metal grids [11] have emerged. Moreover, 1D materials such as carbon nano tubes (CNTs) [12] and metal nanowires [13] have been widely investigated as TCEs for many optoelectronics applications. Despite the progress achieved with those TCE candidates, they have many limitations including chemical and mechanical stability issues, rough surface, and limited light transmittance. Graphene-based TCEs for OSCs have received intensive research interest as excellent candidates to replace ITO due to their superior electrical and optical characteristics in addition to its high chemical and mechanical stability.[14-16] Radio frequency plasma enhanced chemical vapor deposition (RF PECVD) has great potential as an effective approach to synthesize graphene TCEs for optoelectronics.[17, 18] Nonetheless, the high cost, high synthesis temperature, the use of carrier gases and unsustainable, environmentally hazardous carbon sources represent the main drawbacks of RF

PECVD for graphene TCEs. Moreover, the complicated and time-consuming procedures required to transfer graphene onto the transparent (glass/flexible) substrate can damage the film features.[19] Therefore, the abovementioned limitations associated with graphene TCEs-based PECVD need to be addressed before its ubiquitous commercialization.

The direct synthesis of graphene on transparent substrates is a promising strategy to avoid the damage of graphene features upon the associated complex transfer procedures. It also reduces the fabrication cost of the TCE and the whole OSC device. Although a few reports are available on the transfer-free graphene TCEs [17, 18, 20], they have not fully addressed the issues discussed above. Recently, we reported a direct synthesis of graphene TCEs for OSCs on glass by RF PECVD from sustainable plant extract of Pelargonium graveolens. OSCs based on the directly-synthesized graphene TCEs showed a promising performance, but they exhibited low fill factor (*FF*) because of the relatively high sheet resistance (R_s) of graphene, leading to poor carrier collection [21]. Increasing the number of layers reduces R_s of the graphene film, but this leads to a dramatic drop in the film optical transmission and the performance of the OSC device. Thus, the electrical properties of the CVD transfer-free graphene TCEs need to be improved without ruining their optical transmittance for enhanced carrier collection, FF and power conversion efficiency (PCE) of the associated OSCs.

Several approaches have been reported to enhance the electrical conductivity of graphene such as chemical doping, photochemical and plasma associated methods. Nonetheless, doping strategies result in a considerable degradation in the optical transmission and stability of graphene [20]. The hybridization of silver nanowires (AgNWs) and graphene has been reported by many researchers [22-24] to improve the electrical properties of graphene. AgNWs were added to graphene nanosheets prepared by different methods including CVD on metal substrates [25, 26] and exfoliation [27]. Despite enhancing the electrical properties of the resulting hybrid silver nanowires-graphene (AgNWs-Gr) TCEs and the device performance in previous work, [25-27] they included complex synthesis and transfer procedures of graphene onto the AgNWs-coated transparent substrate. To the best of our knowledge, the coupling of AgNWs with transfer-free graphene TCEs has not been reported yet.

Herein, we investigated the possible ways to hybridize AgNWs with the transfer-free graphene TCEs developed from a plant extract using RF-PECVD for OSCs. AgNW networks were spin coated from AgNW dispersions in isopropyl alcohol (IPA) with three concentrations (1, 2, and 3 mg ml⁻¹). Two sets of hybrid electrodes were prepared; AgNWs-Gr, and Gr-AgNWs, where AgNWs were spin coated on top of the bare glass substrate (prior to graphene deposition) and on top of graphene, respectively. For Gr-AgNWs hybrid TCEs, AgNWs provided additional conducting channels connecting the neighboring graphene domains which significantly improved the electrical conductivity of the graphene without reducing its optical transmittance. For instance, spin coating the 1 mg ml⁻¹ concentration AgNW dispersion onto graphene with an original R_s of 1.92 k Ω / \square and transmittance of 73.3%, significantly reduced R_s of the hybrid film to 1.26 k Ω / \square without altering its transmittance (73%). Increasing the concentration of AgNWs to 3 mg ml⁻¹ led the R_s of the Gr-AgNWs3 TCE to drop to 103

 Ω/\Box with transmittance of 66%. Inverted OSCs with a P3HT: PCBM active layer based on pristine graphene TCEs had a PCE of 1.41% and FF of 0.47, while those built on Gr-AgNWs-1 exhibited a PCE of 1.85% and FF of 0.61 which are comparable to the control device on ITO which had a PCE of 2.22% and FF of 0.60. In addition, devices prepared on Gr-AgNWs3 TCEs had an outstanding performance with a PCE of 2.18% and FF reaching 0.63. In the same context, the PM6:Y6-device fabricated on the hybrid TCE exhibited a comparable PCE (9.75%) to that on ITO (10.3%).

For AgNWs-Gr hybrid TCEs, R_s was found to decrease to 1.7 k Ω / \square with 66% optical transmittance at AgNWs dispersion concentration \leq 2 mg ml $^{-1}$ and then increased to 2.4 k Ω / \square with transmittance of 62% for AgNWs3-Gr. OSCs fabricated on AgNWs1-Gr and AgNWs2-Gr exhibited improved performance with a PCE of 1.56% and 1.49% and FF of 0.52 and 0.49, respectively, compared to the pristine graphene due to enhanced electrical conductivity. AgNWs3-Gr based OSCs, exhibited poor performance with a PCE of 1.13% and FF of 0.39 as a result of the increased R_s and low optical transmittance. The growth of graphene nano sheets increased remarkably on top of and close to AgNWs leading to non-uniform film distribution at AgNWs3-Gr with high R_s and low transmittance. It is worth to mention that the deposition temperature of graphene negatively impacted the AgNWs network. Therefore, lower-temperature synthesis of graphene on AgNWs may result in more improvements in the structure of AgNWs-Gr hybrid TCEs and their associated device performance. The obtained data affirm that the developed transfer-free Gr-AgNWs and AgNWs-Gr hybrid TCEs are an advancement towards sustainable, time- and cost-effective production of ITO-free OSCs.

2. Methods

2.1. Preparation of graphene-AgNWs hybrid electrodes

2.1.1. AgNWs/graphene TCE

AgNWs dispersion in isopropyl alcohol (IPA) with a concentration of 20 mg/ml was purchased from ACS Material with an average diameter 40 nm, length of 20 – 60 μm, and purity of 99.5%. A thin layer of AgNWs was prepared on a glass substrate by spin coating. Prior to spin coating of AgNWs, the glass substrate was cleaned in an ultrasonic bath of distilled water with decon90, distilled water, acetone, and IPA for 10 minutes each. The glass substrate was then dried by air gun and left on a pre-heated hot plate at 150 °C for 20 minutes to remove any residues. The substrate was then treated by oxygen plasma for 15 minutes to enhance its hydrophilicity. The AgNW dispersion was diluted by IPA to obtain the optimum concentration. To get a homogeneous layer of AgNWs, the AgNWs dispersion was shaken gently for five minutes and then left for 30 minutes to stabilize before spin coating. The AgNW solutions were spin coated onto the glass substrates at 3000 rpm for 60 s to produce AgNWs-network coating. Then, the AgNWs-coated glass substrates were dried on a hot plate at 90 °C for 15 minutes before they were moved to the RF PECVD reactor to deposit graphene films. 1 ml of Pelargonium graveolens (geranium oil), purchased from Australian botanical products (ABP), was used as a sustainable carbon source. Geranium oil was utilized as received without any pre-treatment or purification. More details

on the major constituents of geranium oil can be found in our previous work ref. [21]. The substrate was heated up to 600 °C under a vacuum of 4×10^{-2} mb and then treated by 500 W air plasma for two minutes. Then, the monomer vapor was allowed to enter the reactor and after the monomer pressure stabilized, 200 W RF power was applied for 2 minutes to synthesize graphene films. Finally, the reactor was cooled down to room temperature and the AgNWs-graphene hybrid TCE was ready to use.

2.1.2. Graphene/AgNWs TCE

Graphene/AgNWs TCEs were synthesized in a reverse manner to AgNWs/graphene discussed above through spin coating AgNWs dispersion on top of graphene films. Graphene films were prepared under the same conditions as discussed earlier.

2.2. Characterization of AgNWs-graphene hybrid electrodes

Raman spectroscopy (Reinshaw Raman Microscope, 514 nm laser) was used confirm growth of graphene. JEOL Field Emission scanning electron microscope (SEM) was used to investigate the morphology of the developed films. The sheet resistance of the investigated films was studied using four-point probe method as discussed in our previous work,[21] while Ellipsometer (J.A. Woollam Co. Inc. M-2000D) was used to measure their optical transmission. The purity and quality of the prepared films were investigated using a Kratos AXIS SUPRA PLUS X ray photoelectron spectrometer (XPS) with a monochromatic Al Kα X-ray source (hv = 1486.6 eV) operated at and 12 kV anode potential and 10 mA emission current. Transmission electron microscope (TEM) (Hitachi HT7700 TEM equipped with LaB6 filament operating at 120 kV) was utilized to study structural features such as the number, interspacing and stacking of graphene layers within the TCE films.

2.3. Device fabrication and characterization

Organic photovoltaic (OPV) devices studied in the present work adopted the inverted geometry with the structure TCE/ZnO/active layer/ MoO3/Ag. Prior to device fabrication, the graphene-based TCEs were treated by air plasma for 30 seconds at 5 W RF power, while ITO substrates were treated by oxygen plasma for 8 minutes at 25 W. The plasma treatment makes the surface of the TCE more hydrophilic to get a uniform coating of ZnO layer [28]. ZnO sol-gel was prepared through dissolving 0.109 gm of Zn-Acetate in 2-methoxyethanol (purity %, 1 ml, Sigma Aldrich) with 32 µl of ethanolamine as additive [29]. ZnO electron transport layer (ETL) was obtained by spin coating ZnO sol-gel on top of TCE at 3000 rpm for 60 seconds then thermally annealed at 150 °C for 10 minutes in air. In order to reduce the influence of rough surface of either graphene or AgNWs and to avoid short circuits, the deposition of ZnO was repeated three times [30]. The active blend was prepared by dissolving P3HT: PCBM (1: 0.8 wt/wt) in Chlorobenzene with 25 mg ml⁻¹ overall concentration at 50 °C overnight inside a N₂-filled glovebox. The active layer was spin coated at 2000 rpm for 30 s on ZnO ETL followed by 10 minutes thermal annealing at 120 °C on a hot plate in an inert atmosphere. For the

devices with P3HT: PC₇₀BM active layer, the preparation procedure was exactly the same as that with P3HT: PCBM counterparts. In the case of PM6: Y6 based OPVs, a total concentration of 16 mg/ml with donor to acceptor ratio of 1: 1.2 was dissolved in chloroform and 0.5% v/v 1-chloronaphthalene solvent additive at 50 °C overnight inside the glovebox. PM6: Y6 was spin coated at 3000 rpm for 35 s onto ZnO. The substrates were then moved to a 12A4 HIND HIVAC thermal evaporation unit to deposit 3.5 nm MoO₃ and 130 nm Ag as the hole transport layer (HTL) and anode, respectively. The active area of the produced devices was decided as 4 mm² using a deposition mask. The current density-voltage (J-V) characteristic curves for the investigated devices were recorded under 100 mW cm⁻² illumination of AM1.5 G solar simulator (ABET Sunlite) using a Keithley source measure unit (model: 2636A) and a custom-made test board. A reference Si solar cell was used to calibrate the light intensity of the solar simulator. The J-V data were collected in ambient conditions without device encapsulation.

3. Results and discussion

The Raman spectra of pristine graphene, hybrid AgNWs-Gr, and Gr-AgNWs films are shown in Fig. 1. The 2D peak at ~2670 cm⁻¹ is characteristic for the graphene (2-dimensional hexagonal carbon lattice) and accounts for second order zone-boundary phonons [31]. The broadened 2D peak indicates the formation of few to multi-layer graphene films.[32] The G peak (~ 1560 cm⁻¹) is attributed to the characteristic in-plane E2g vibration of sp² hybridized carbon. The imperfections within the synthesized graphene structure, including vacancies, wrinkles and dislocations are represented by the D peak (~1335 cm⁻¹) and other low-intensity peaks such as D' (1609 cm⁻¹), D+G (~2915 cm⁻¹) and 2D' (~3210 cm⁻¹). The ratio between the intensity of 2D and G peaks is correlated to the number of graphene layers in the sample, while the ratio between I_D/I_G indicates the structural disorders.[33] The higher the value of I_D/I_G, the more defects are present in the graphene lattice. Also, the I_{2D}/I_G ratio increases as the number of graphene layers decreases [34, 35]. The relatively low values of I_{2D}/I_G (0.69) and I_D/I_G (0.88) for the pristine graphene reveal the formation of a few-layer graphene with moderate to low defect concentration which was confirmed by other characterization methods as discussed later in this paper.

The Raman spectra of the Gr-AgNWs and AgNWs-Gr hybrid films showed the same peaks as pristine graphene, but with varying ratios as shown in Fig. 1(b and d). For Gr-AgNWs films, it can be observed (Fig. 1(b)) that the ratio of I_{2D}/I_G remained almost unchanged with changing the spin coated concentration of the AgNWs dispersion compared to that of pristine graphene. This result is reasonable as the number of graphene layers should not change when AgNWs are coated on the sample top. On the other hand, the I_D/I_G for Gr-AgNWs films increased from 0.88 (for pristine graphene) and reached 1.03 and 1.07 at AgNWs concentrations of 1-2 mg/ml and 3 mg/ml, respectively.

In the case of AgNWs-Gr hybrid films, both I_{2D}/I_G and I_D/I_G were found to vary with AgNWs concentration (Fig. 1(d)). Although I_{2D}/I_G did not change much at AgNWs concentrations of 1 mg ml⁻¹, it dropped to 0.67, and 0.63 at concentrations of 2 and 3 mg ml⁻¹, respectively. The drop in I_{2D}/I_G indicates a higher number of graphene layers compared to graphene films formed on bare glass. The

increase in the number of graphene layers may indicate catalytic activity of AgNWs towards graphene synthesis by PECVD. Furthermore, the high ratios of I_D/I_G for the AgNWs-Gr samples indicate increased disorders in graphene structures such as dislocations and discontinuities, as affirmed by the SEM and TEM data.

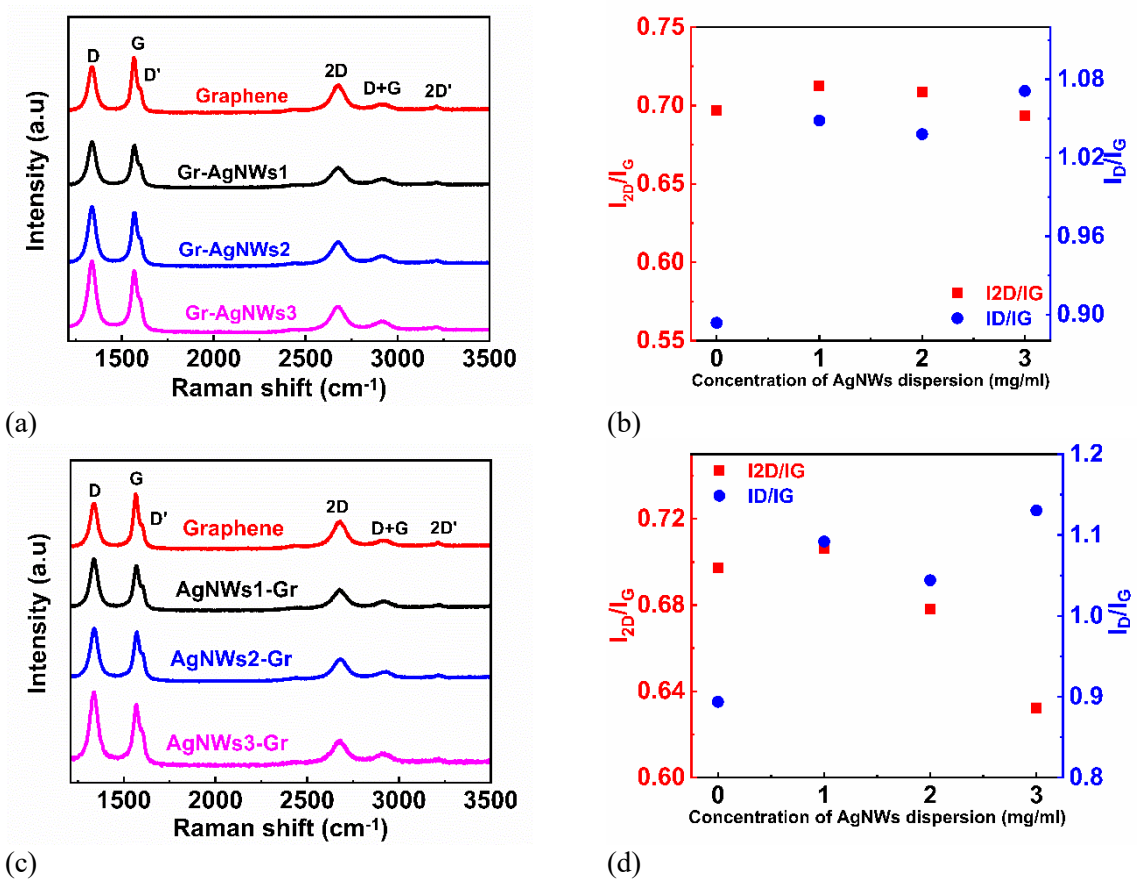
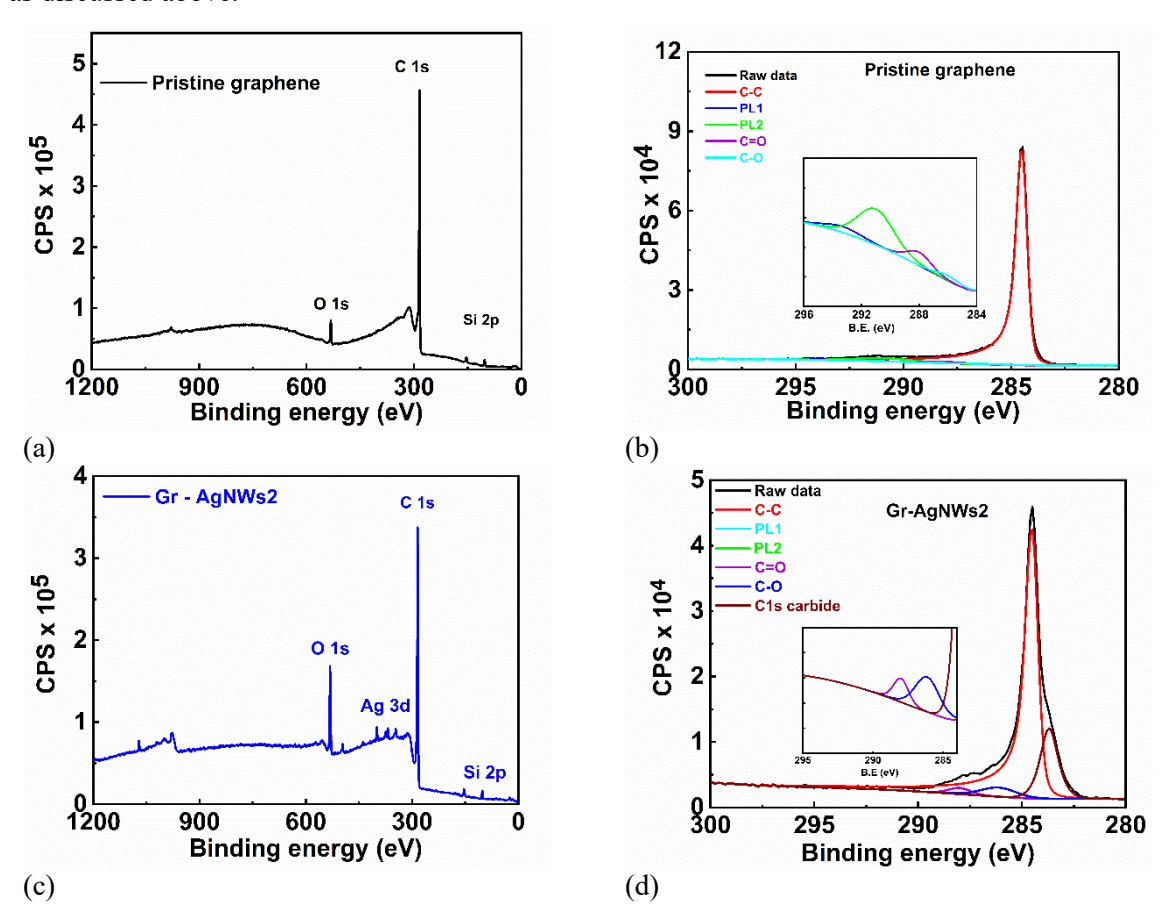
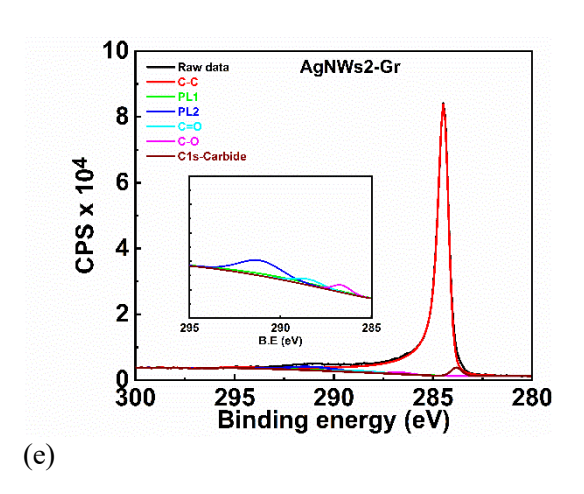


Fig. 1 Raman spectra for pristine graphene and hybrid Gr-AgNWs (a) and AgNWs-Gr (c). The variation of I_{2D}/I_G and I_D/I_G for the investigated Gr-AgNWs (b) and AgNWs-Gr (d).

For investigating the structural purity and the chemical composition of the synthesized pristine and hybrid graphene films, XPS characterization was performed. Fig. 2 depicts XPS spectra for pristine graphene, AgNWs2-Gr, and Gr-AgNWs2 samples. More details on the associated XPS peaks for the investigated samples are given in table 1. The survey scan for pristine graphene shows a predominant high intensity C 1s peak at binding energy (B.E) ~ 284.5 eV with 94.96 atomic percentage (At%). In addition, two smaller peaks were observed at a B.E of 532.5 eV and 102.5 eV representing O 1s and Si 2p, with 2.56 At% and 2.48 At%, respectively. The high percentage of C in the XPS spectrum reveals the high purity of the prepared graphene. The emergence of O 1s may be attributed to either the interaction of ambient oxygen with the active sites within the graphene lattice or due to oxygen-containing components in the Pelargonium graveolens [36, 37]. The minor Si 2p peak at a B.E. of 102.5 eV is ascribed to the substrate surface. More details on Si 2p peak can be found in Fig. S1. The C 1s region, deconvoluted using CasaXPS software, showed a main peak attributed to the sp² hybridized carbon at 284.5 eV.[38, 39] Other peaks describing C-O and C=O and the Plasmon loss features due to

graphitic carbon were also observed [40] more details can be found in our previous work [21]. For the hybrid Gr-AgNWs films (Fig. 2(c)), a minor Ag 3d peak with a minimum contribution to the whole spectrum (0.14 At %) was observed at B.E. of 368.6 eV. A high intensity O 1s and N 1s peaks were observed at B.E. 531.6 eV and 399.6 eV, respectively. The O 1s and N 1s peaks may be attributed to the residual polyvinylpyrrolidone (PVP) and glycerol attached with AgNWs.[41] The high resolution scan of the Ag 3d peak reveals two peaks at B.E. of 368.3 eV (Ag $3d_{5/2}$) and 374.3 eV (Ag $3d_{3/2}$) as shown in Fig. S1(d) which is in good agreement with literature [41]. The XPS spectrum for the AgNWs2-Gr hybrid film was found to be similar to that of the pristine graphene without any peaks for Ag. The absence of Ag peaks for this sample can be attributed to the higher number of graphene layers which prevents the incident photons from travelling deeper into the sample. The increased number of layers of graphene synthesized on top of AgNWs was confirmed by TEM images and optical transmission measurements and reflected on the photovoltaic parameters of the OSCs built on these TCEs. Moreover, the SEM images for AgNWs-Gr samples revealed that the growth of graphene nanosheets on top of and close to the AgNWs was much more than anywhere else on the substrate. This can explain the emergence of minor peaks such as Si 2p which is associated with the substrate surface as discussed above.





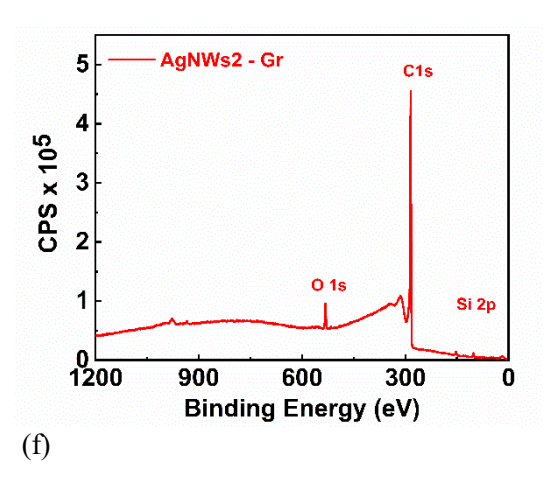


Fig. 2 XPS survey data for pristine graphene (a), Gr-AgNWs2 (c), and AgNWs2-Gr (f). Deconvoluted high resolution scan of C 1s peak for graphene (b), hybrid Gr-AgNWs2 (d), and AgNWs2-Gr (e).

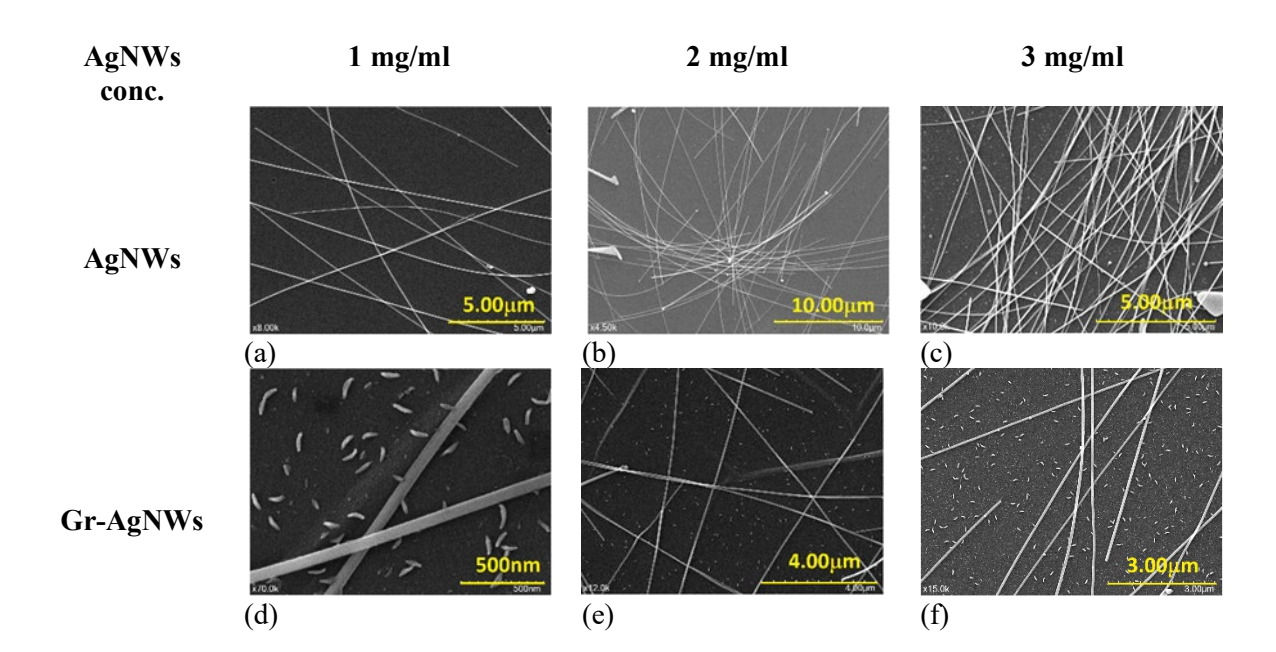
Table 1

The position and atomic percentage of the different XPS peaks for the investigated samples.

Sample	C 1s		O 1s		Ag 3d		N 1s		Si 2p		Na 1s		Ca 2p	
	B.E. (eV)	(At %)	B.E. (eV)	(At%)	B.E. (eV)	(At%)	B.E. (eV)	(At%)						
Graphene	284.5	94.96	532.5	2.56		0		0	102.5	2.48		0		0
Gr- AgNWs2	284.5	80.65	531.6	13.04	368.6	0.14	399.6	1.89	101.6	3.35	107.6	0.5	346.66	0.42
AgNWs2- Gr	284.3	94.83	531.3	3.35		0	399.3	0.54	101.3	1.28				

The morphology of the AgNWs, AgNWs-Gr and Gr-AgNWs on glass substrates was investigated by SEM. Fig. 3(a - c) reveals the formation of interconnecting networks of AgNWs on glass with a significant increase in the surface density of AgNWs as the concentration of AgNWs dispersion increases. In addition, the agglomeration and aggregation of AgNWs can be easily observed at higher concentrations (Fig. 3(b & c)). The dimensions of the spin-coated AgNWs can be confirmed with an average diameter of 40 nm and lengths ranging from 20 to 60 µm (Fig. S2). On the other hand, the configuration of AgNWs on top of graphene films is shown in Fig. 3(d - f). These images show graphene films with the emergence of vertical graphene nano-islands which is in close agreement with previous work [21]. More details on the vertical graphene nano-islands were obtained by AFM images in Fig. S3 and table S1. It can also be noticed that AgNWs reside within these graphene nano-islands (Fig. 3(d-f)). More interestingly, AgNWs on graphene were found to be more homogeneously distributed with no noticeable agglomeration and lower surface density than AgNWs on bare glass at the same concentrations of AgNWs dispersion. These observations were reflected on the optical and electrical characteristics of the resulting Gr-AgNWs hybrid TCEs and the photovoltaic performance of the organic photovoltaic (OPV) devices based on them as discussed later in this manuscript. For AgNWs-Gr hybrid films, the formation of graphene nanosheets on top of AgNWs was also achieved

(Fig. 3(g-i)). It is obvious that the growth of graphene nano-islands markedly increased close to and on AgNWs which resulted in non-uniform coverage of graphene films on the AgNWs-coated glass. This may be an indication of catalytic activity of these metallic nanowires towards graphene synthesis. The growth of graphene nanosheets enhanced with increasing concentration of AgNWs dispersion. Moreover, the AgNWs network within the hybrid AgNWs-Gr TCEs experienced some deformation during the deposition of graphene which may be attributed to the reaction temperature (600 °C) and/or the RF plasma power (200 W). This deformation may be avoided at lower deposition temperatures and RF power for more enhancement of the properties of the hybrid AgNWs-Gr films. TEM images (Fig. 3(j-l)) provided an in-depth insight on structural features of the investigated samples. The interlayer spacing for the pristine and hybrid graphene samples was found to be 0.34 nm which is in excellent agreement with the theoretical value (0.33 nm) [42, 43]. Higher resolution TEM images for calculating the interlayer spacing can be found in Fig. S4. It is obvious that the number of graphene layers increased for the AgNWs-Gr hybrid sample with respect to pristine graphene and Gr-AgNWs, confirming the Raman data (Fig. 1(b & d)).



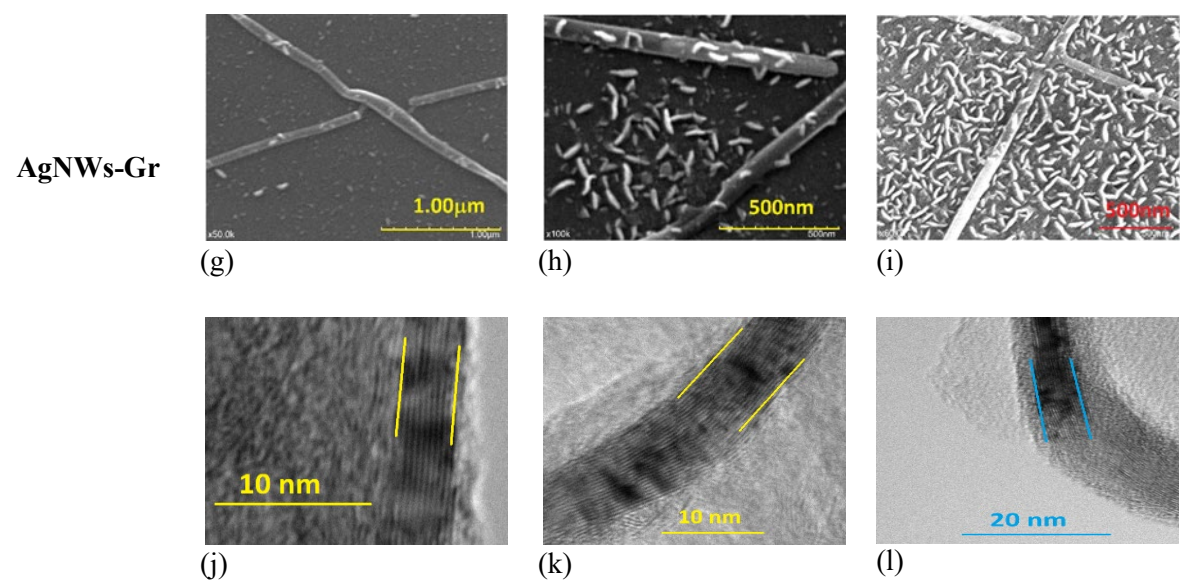


Fig. 3 SEM images for AgNWs (a-c), Gr-AgNWs (d-f), and AgNWs-Gr (g-i) on glass substrates. (j-l) Representative TEM images for pristine graphene (j), AgNWs2-Gr (k), and Gr-AgNWs2 (l).

Fig. 4 and table 2 show the variation of sheet resistance for the investigated TCEs. It can be observed that AgNWs greatly impacted the sheet resistance of the hybrid TCEs compared to the pristine graphene counterparts. Adding AgNWs on to the graphene films significantly improved their electrical properties and sharply reduced the sheet resistance as depicted in Fig. 4(a) and table 2. Although the AgNWs network on the glass from the 1 mg ml⁻¹ dispersion had a large R_s of 0.5 M Ω / \square (Fig. S5), it caused the R_s of the Gr-AgNWs1 hybrid film to drop (1.26 k Ω/\Box) compared to the pristine graphene (1.92 k Ω / \square), with almost no change in the optical transmittance of the resulting film. This enhancement can be attributed to the additional conductive pathways created by AgNWs which facilitate electron transport through the film.[44] At higher concentrations of AgNWs dispersion (2 and 3 mg ml⁻¹), the surface density of the AgNWs mesh on top of graphene increased, providing more conductive ways and more connections to the graphene domains leading to lower R_s of 374 Ω/\Box and 103 Ω/\Box for Gr-AgNWs2 and Gr-AgNWs3, respectively. Interestingly, the Rs values of the AgNWs mesh spin coated on bare glass at AgNWs dispersion concentrations of 2 and 3 mg ml⁻¹ were 198 Ω / \Box for AgNWs2 and 56 Ω / \Box for AgNWs3 which are approximately one half of their respective values when coated on graphene. This can be explained as AgNWs tend to have more aggregations and higher surface density when spin coated on bare glass than graphene, which is in good agreement with SEM images (Fig. 3). In addition, these high aggregations led to short circuits in OPV devices developed on AgNWs spin coated on bare glass and will be discussed later.

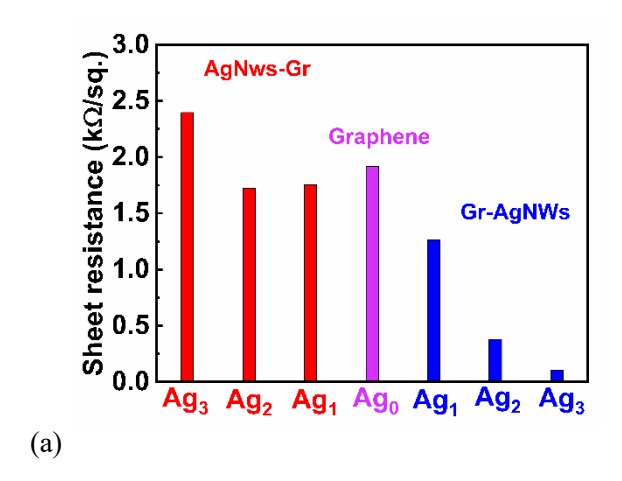
When graphene films were grown onto AgNWs-coated glass, R_s of the resulting AgNWs-graphene hybrid TCEs decreased to $\sim 1.7~k\Omega/\Box$ at AgNWs dispersion concentration $\leq 2~mg~ml^{-1}$. AgNWs3-Gr had a higher R_s of $2.4~k\Omega/\Box$ although it had a higher number of layers than AgNWs1-Gr and AgNWs2-Gr as confirmed by Raman and optical transmission data. The reduced R_s of AgNWs-Gr at lower concentrations of AgNWs dispersion compared to pristine graphene may be attributed to the

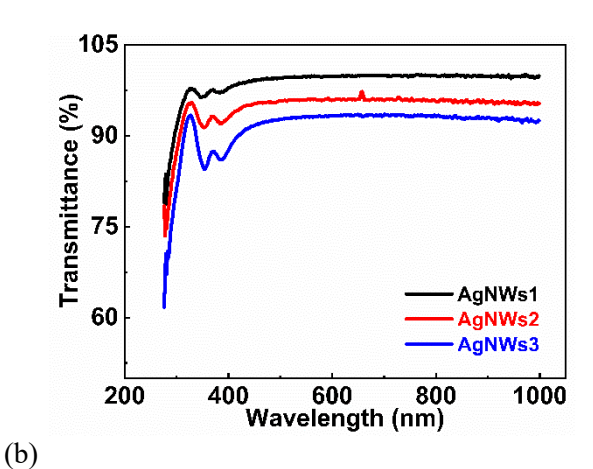
connections of AgNWs to graphene domains. The degradation in the electrical conductivity for AgNWs3-Gr could be ascribed to the non-uniform distribution of graphene nanosheets on the substrate as confirmed by the SEM images. The irregular configuration of graphene nanosheets and the increased defect concentration- as confirmed by Raman data- within the film explain the high R_s of AgNWs3-Gr hybrid TCE.. Also, it is notable that AgNWs within AgNWs-Gr films exhibited deformation during heating within the CVD chamber. Therefore, lower-temperature synthesis of graphene on AgNWs may enhance the quality of AgNWs-Gr hybrid TCEs and their associated device performance.

The optical transmittance data (table 2) reveal that Gr-AgNWs1 hybrid film had a transparency comparable to that of the pristine graphene (73% cf.73.3%) (Fig. S6). This minor change is due to the low surface density of the AgNWs1 network, allowing its transmission to reach 99%. The transmission of the Gr-AgNWs reached 66% with increasing concentration of the AgNWs dispersion as a result of the higher surface density of the AgNWs mesh on top of graphene film. For AgNWs-Gr TCEs, the drop in optical transmission of the hybrid films was greater compared to its corresponding Gr-AgNWs counterparts. The AgNWs1-Gr and AgNW2-Gr films had almost similar optical transmission of ~66% which confirms their similar R_s as discussed above. For AgNW3-Gr, its optical transmission dropped to 62% due to the high surface density of the AgNWs3 mesh which increased the growth of graphene nano sheets above and close to AgNWs as clear in Fig. 3(i). Furthermore, the high number of graphene layers makes the film less transparent which is in agreement with the Raman data. In addition, the figure of merit (FoM) of the investigated TCE films was calculated using R_s and transmittance (T) according to equation1 below [45]:

$$FoM = \frac{188.5}{R_s (T^{-0.5} - 1)}$$
 (1)

It can be observed that the FoM for the Gr-AgNWs hybrid films increased as the concentration of AgNWs increased, but dropped for AgNWs-Gr films as discussed above with optical transmittance and $R_{\rm s}$ variation.





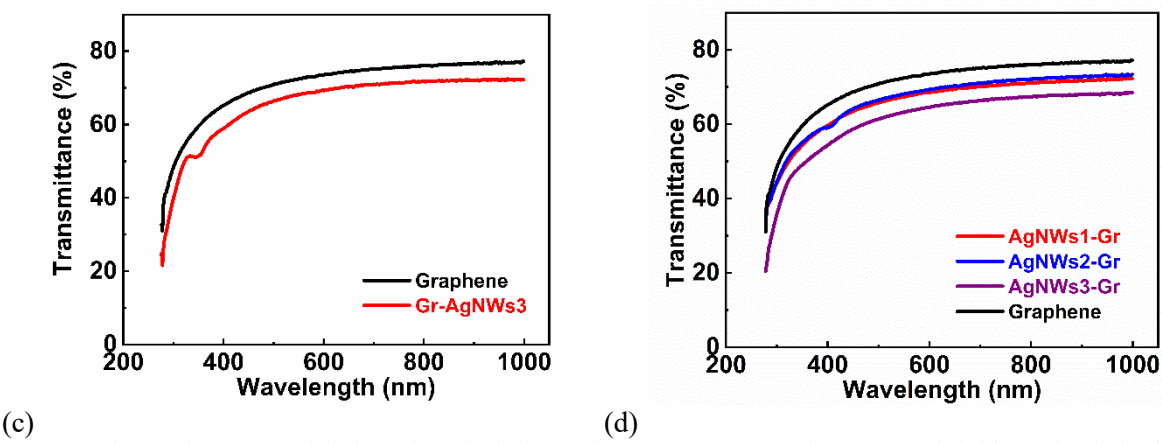


Fig. 4 (a) Sheet resistance, R_s of the investigated pristine graphene, Gr-AgNWs, and AgNWs-Gr hybrid samples. b-d) The variation of optical transmission with the wavelength of the incident light for AgNWs on bare glass (b), graphene and Gr-AgNWs3 (c), and graphene and AgNWs-Gr films (d).

Table 2

The sheet resistance and optical transmission of the investigated TCE samples.

TCE	Sheet resistance (k□/sq.)	Transmittance at 550 nm (%)	Figure of merit (FoM)
Graphene	1.92	73.3	0.58
AgNWs1	500	99	0.075
AgNWs2	0.198	95	36.64
AgNWs3	0.056	93	91.2
Gr - AgNWs1	1.26	73	0.88
Gr – AgNWs2	0.374	69	2.47
Gr – AgNWs3	0.103	66	7.92
AgNw1-Gr	1.752	66	0.47
AgNWs2-Gr	1.722	65	0.45
AgNWs3-Gr	2.4	62	0.29

The photovoltaic performance of the devices based on the prepared TCEs and ITO was analyzed from the J-V curves (Fig. 5). These OPV devices employed P3HT: PCBM as the photoactive blend. Fig. 5(a) shows the J-V curves of the devices built on the as-synthesized graphene and the reference (ITO) TCEs. The values of their photovoltaic parameters are listed in table 3. It can be observed that the device based on pristine graphene exhibited almost 65% of the PCE of the reference counterpart with comparable open-circuit voltage (V_{OC}). The lower PCE (1.41%) of the device fabricated on graphene compared to the reference device (PCE = 2.22%) is attributed to its lower FF (0.47) and short-circuit current density (J_{SC}). The reduced FF and J_{SC} can be assigned to the higher R_s of graphene relative to ITO as discussed above. Fig. 5(b) reveals the positive impact of adding AgNWs to graphene on the photovoltaic performance of the device even at the low concentration of AgNWs. The spin coating of AgNWs with concentration of 1 mg ml⁻¹ increased the FF of the device from 0.47 (graphene) to 0.61 (Gr-AgNWs1) although the device based on AgNWs1 TCE showed a resistor-like behavior. Fig. 5(c) depicts the J-V characteristics of OPVs based on the hybrid graphene-AgNWs TCEs

with three concentrations of the spin coated AgNWs dispersion; 1, 2, and 3 mg ml⁻¹. The addition of AgNWs on top of graphene significantly improved the photovoltaic performance of the resulting OPVs compared to the pristine graphene. The addition of AgNWs resulted in a remarkable enhancement with the FF of the device reaching 0.63 when increasing AgNWs concentration to 3 mg ml⁻¹. This improvement can be due to the reduction in the sheet resistance and the enhanced morphology of the hybrid TCEs which improved carrier collection. In addition, it can be observed that the J_{SC} for the devices built on the hybrid TCEs at different AgNWs concentrations is higher than that for pristine graphene which can be ascribed to their enhanced electrical conductivity and comparable optical transmittance to graphene. Furthermore, the J_{SC} for the hybrid TCEs-based devices increases as the AgNWs increased due to the reduced sheet resistance which compensates for the drop in optical transmittance. Adding AgNWs onto graphene made it more competitive to the standard ITO electrode. Fig. 5(d) and table 3 reveal that the device based on Gr-AgNWs3 had an outstanding performance with a comparable PCE (2.18%) due to the higher FF of 0.63 (a maximum FF of 0.65 was also achieved) to the reference device (on ITO). The remarkable performance of the device fabricated on the Gr-AgNWs3 hybrid TCE can be assigned to the low sheet resistance and improved surface morphology. In addition, the increased area of contact (interface) between the active layer and the bottom electrode, as demonstrated by AFM images (Fig. S7), enhanced the collection of the photo-generated electrons leading to a higher FF. It can be observed that although the device performance improves with increasing the FoM of the TCE material, this enhancement does not vary linearly with the FoM which is in a good agreement with literature [20, 21, 46]. It is worth mentioning that adding higher concentration of AgNWs (>3 mg ml⁻¹) onto graphene can lead to device failure as a result of shorts and reduced optical transmittance of the resulting hybrid TCEs. On the other hand, OPV devices fabricated on AgNWs TCEs showed very poor performance at low concentration (1 mg ml⁻¹) or exhibited shortcircuiting at higher concentrations (Fig. 5(e)). The deteriorated performance at 1 mg ml⁻¹ (Fig. 5(b)) is assigned to the extremely high Rs of the AgNWs1 TCE (table 2), while in the case of the higher concentrations (2 and 3 mg ml⁻¹), the aggregation of AgNWs on bare glass (Fig. 3b&c) led to the penetration of the nanowires to the top layers of the device and made direct contact with the top metal electrode. Further procedures such as hot rolling [47] may be needed to avoid the short-circuiting in cases of high concentrations of AgNWs on bare glass.

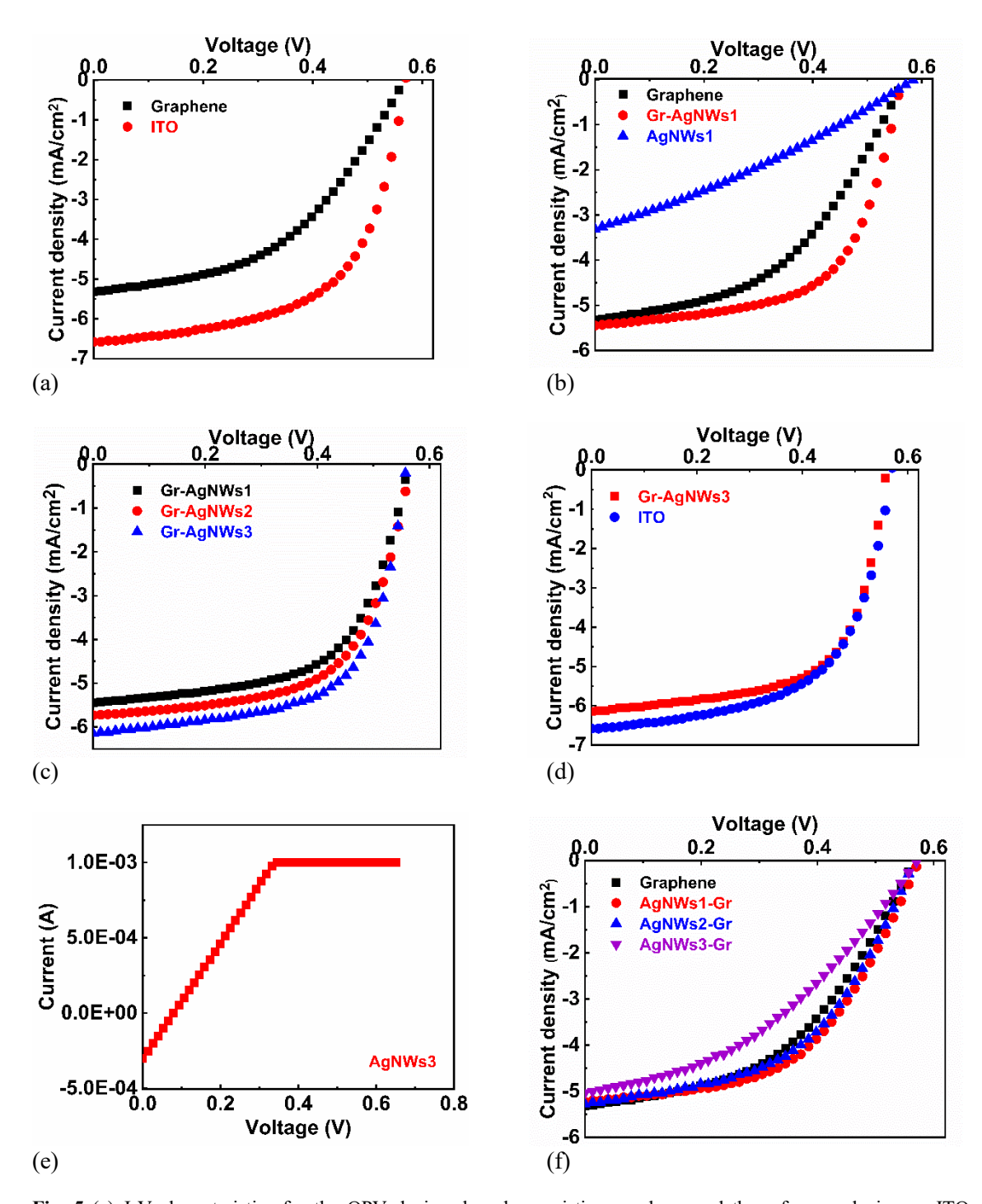


Fig. 5 (a) J-V characteristics for the OPV devices based on pristine graphene and the reference device on ITO. b) Comparison of the photovoltaic performance of the devices developed on AgNWs1, graphene, and Gr-AgNWs1. c &f) The variation of the J-V curves for OPV devices fabricated on the hybrid Gr-AgNWs (c) and AgNWs-Gr (f) with the concentration of the spin coated AgNWs dispersion. d) A comparison between the performance of the champion device on the developed Gr-AgNWs3 TCE and ITO counterpart. e) The short circuit within the device developed on AgNWs3 (on bare glass) TCE due to the large agglomeration of AgNWs.

On the other hand, the devices built on AgNWs-Graphene TCEs demonstrated a good performance at AgNWs concentrations of 1 and 2 mg ml⁻¹, but the performance dropped significantly at higher AgNWs concentration (Fig. 5(f)). The PCEs of the devices based on AgNWs1-Gr and AgNWs2-Gr electrodes were higher than that of the device prepared on pristine graphene due to the enhanced J_{SC} and FF as

listed in table 3. The improved J_{SC} and FF of these devices originate from the reduced R_s of the hybrid AgNWs-Gr TCEs at low concentrations. At higher concentration of AgNWs (3 mg ml⁻¹), the PCE dropped to 1.13% with an FF of 0.39 compared to AgNWs1-Gr and AgNWs2-Gr TCEs which achieved PCEs of 1.56% and 1.49% and FF_s of 0.52 and 0.50, respectively. The deteriorated photovoltaic performance of this device is attributed to the low optical transmission and high R_s of the AgNWs3-Gr TCE. Moreover, the non-uniform morphology of this electrode may increase the leakage current of the device resulting in a dramatic drop in FF and J_{SC} . Subsequently, the reduced photo-generation and collection of the charge carriers reduced the J_{SC} , FF, and PCE of the device. Also, the deformation of AgNWs network within AgNWs-Gr films during graphene deposition can limit the improvement or have negative impact on the resulting hybrid film. Our future research focuses on reducing the synthesis temperature of the reported sustainable and transfer-free graphene to avoid any damage to the AgNWs underneath and to make the hybrid electrode more promising.

Table 3 The photovoltaic parameters of the OPV devices developed on the investigated TCEs using P3HT: PCBM as an active layer. The values in parentheses represent the device with the best PCE.

TCE	Active layer	$ m J_{SC}$	Voc	FF	PCE
		(mA/cm ²)	(V)		(%)
Graphene		5.20 ± 0.47	0.56 ± 0.01	0.48 ± 0.01	1.37 ± 0.05
		(5.32)	(0.56)	(0.47)	(1.41)
Gr-AgNWs1		5.34 ± 0.34	0.56 ± 0.01	0.59 ± 0.04	1.74 ± 0.14
		(5.45)	(0.56)	(0.61)	(1.85)
Gr-AgNWs2	P3HT:PCBM	5.59 ± 0.19	0.55 ± 0.01	0.61 ± 0.01	1.88 ± 0.14
		(5.73)	(0.56)	(0.62)	(1.99)
Gr-AgNWs3		5.79 ± 0.45	0.56 ± 0.01	0.64 ± 0.01	2.07 ± 0.14
		(6.15)	(0.56)	(0.63)	(2.18)
AgNWs1-Gr		5.32 ± 0.43	0.58 ± 0.02	0.49 ± 0.05	1.50 ± 0.12
		(5.23)	(0.58)	(0.52)	(1.56)
AgNWs2-Gr		5.38 ± 0.30	0.57 ± 0.01	0.48 ± 0.03	1.46 ± 0.09
		(5.28)	(0.56)	(0.50)	1.49
AgNWs3-Gr		4.94 ± 0.21	0.58 ± 0.02	0.36 ± 0.05	1.03 ± 0.18
		(5.03)	(0.58)	(0.39)	(1.13)
ITO		6.30 ± 0.37	0.56 ± 0.01	0.59 ± 0.01	2.10 ± 0.14
(Reference)		(6.58)	(0.56)	(0.60)	2.22
Gr-AgNWs3	P3HT:PC ₇₀ BM	6.90 ± 0.15	0.55 ± 0.01	0.60 ± 0.01	2.28 ± 0.09

		(7.0)	(0.55)	(0.61)	(2.33)
ITO		6.95 ± 0.24	0.57 ± 0.01	0.58 ± 0.02	2.30 ± 0.06
(Reference)		(7.11)	(0.57)	(0.57)	2.33
Gr-AgNWs3		21.07 ± 0.66	0.77 ± 0.01	0.58 ± 0.01	9.45 ± 0.51
	PM6:Y6	(21.4)	(0.77)	(0.59)	(9.75)
ITO		21.35 ± 0.94	0.76 ± 0.02	0.59 ± 02	9.67 ± 0.81
(Reference)		(22.5)	(0.78)	(0.59)	(10.3)

To check the versatility of the developed Gr-AgNWs hybrid TCEs, OSCs with two different photoactive layers based on PM6:Y6 and P3HT: PC₇₀BM were fabricated on the best-performing TCE (Gr-AgNWs3) and compared to ITO. The variation of the photovoltaic parameters of the devices with different active layers is summarized in table 3. Moreover, the J-V characteristic curves for the devices with the highest PCE are shown in Fig. S8. The obtained results (Fig. S8 and table 3) demonstrated that the performance of the OPV devices developed on the Gr-AgNWs hybrid TCE is comparable to that of ITO counterparts similar to that with P3HT: PCBM active layer.

4. Conclusion

Efficient transfer-free graphene-AgNWs hybrid TCEs for OPVs were developed from a sustainable resource, by RF-PECVD. The electrical conductivity of hybrid Gr-AgNWs films was significantly improved by spin coating AgNWs onto graphene, with the enhancement being more pronounced at higher concentrations of AgNWs dispersion. Additionally, the vertically-oriented graphene nanosheets suppressed the influence of the rough surface of AgNWs. Therefore, P3HT:PCBM-based OPV devices fabricated on Gr-AgNWs had a comparable PCE (2.18 %) and FF (0.63) to their ITO counterpart (PCE of 2.22% and FF of 0.60), whereas those built on AgNWs exhibited poor or deteriorated performance. The higher FF can be due to the increased contact area between the hybrid Gr-AgNWs TCE and the active layer of the device which improved carrier collection. Also, PM6:Y6-device developed on the hybrid Gr-AgNWs TCE demonstrated a competitive PCE (9.75%) to ITO-counterpart (10.3%). On the other hand, the growth of CVD graphene on AgNWs-coated glass caused a drop in the sheet resistance of the AgNWs-Gr film at low concentrations (≤ 2 mg ml⁻¹) of AgNWs dispersion, but R_s increased at the higher concentration. The growth of graphene nanosheets was found to increase on top of and close to the AgNWs leading to a non-uniform distribution of graphene. Nonetheless, the AgNWs-Gr TCEs developed at low concentrations improved the device performance due to the reduced R_s compared to pristine graphene. Consequently, this work represents a remarkable advancement towards the rapid, cheap, and clean synthesis of graphene-based TCEs for OPVs which makes these renewable energy technologies more sustainable.

Supporting information

Additional XPS data fitting of Si 2p and Ag 3d peaks, SEM showing the dimensions of AgNWs, AFM images and Table for rms surface roughness of pristine graphene and Gr-AgNWs, TEM image demonstrating the number of graphene layers and interlayer spacings, four-point probe data AgNWs on glass, optical transmittance for graphene Gr-AgNWs1 and Gr-AgNWs2, 2D and 3D AFM images of ZnO-coated Gr-AgNWs, and J-V characteristics of P3HT: PC₇₀BM and PM6: Y6 OPVs on Gr-AgNWs3 and ITO.

Acknowledgement

Michael S. A. Kamel would like to acknowledge the financial support by the college of Science and Engineering, James Cook University (JCU), Townsville, Australia through JCUPRS scholarship. We acknowledge Dr Olexandra Marenych, CMM UQ for the TEM data acquisition.

Conflicts of interest

The authors declare no conflict of interest.

Data Availability Statement

The data that support the findings of this study are available from the corresponding author upon request.

References

- [1] H. Cui, W. Song, B. Fanady, R. Peng, J. Zhang, J. Huang, Z. Ge, Flexible ITO-free organic solar cells over 10% by employing drop-coated conductive PEDOT: PSS transparent anodes, Science China Chemistry 62(4) (2019) 500-505.
- [2] S. Jung, H. Kim, J. Lee, G. Jeong, H. Kim, J. Park, H. Park, Bio-Inspired Catecholamine-Derived Surface Modifier for Graphene-Based Organic Solar Cells, ACS Applied Energy Materials 1(11) (2018) 6463-6468.
- [3] J. Du, D. Zhang, X. Wang, H. Jin, W. Zhang, B. Tong, Y. Liu, P.L. Burn, H.-M. Cheng, W. Ren, Extremely efficient flexible organic solar cells with a graphene transparent anode: Dependence on number of layers and doping of graphene, Carbon 171 (2021) 350-358.
- [4] E. Keyvani-Someh, Z. Hennighausen, W. Lee, R.C.K. Igwe, M.E. Kramdi, S. Kar, H. Fenniri, Organic Photovoltaics with Stacked Graphene Anodes, ACS Applied Energy Materials 1(1) (2018) 17-21.
- [5] D.S. Hecht, L. Hu, G. Irvin, Emerging transparent electrodes based on thin films of carbon nanotubes, graphene, and metallic nanostructures, Advanced materials 23(13) (2011) 1482-1513.
- [6] M.-S. Chae, T.H. Lee, K.R. Son, Y.W. Kim, K.S. Hwang, T.G. Kim, Electrically-doped CVD-graphene transparent electrodes: application in 365 nm light-emitting diodes, Nanoscale Horizons 4(3) (2019) 610-618.
- [7] Y. Wang, Q. Chen, G. Zhang, C. Xiao, Y. Wei, W. Li, Ultrathin Flexible Transparent Composite Electrode via Semi-embedding Silver Nanowires in a Colorless Polyimide for High-Performance Ultraflexible Organic Solar Cells, ACS Applied Materials & Interfaces 14(4) (2022) 5699-5708.

- [8] J. Wan, Y. Xia, J. Fang, Z. Zhang, B. Xu, W. Jinzhao, L. Ai, W. Song, K. Hui, X. Fan, Y. Li, Solution-Processed Transparent Conducting Electrodes for Flexible Organic Solar Cells with 16.61% Efficiency, Nano-Micro Letters 13 (2021).
- [9] Y.S. Song, N.J. Seong, K.J. Choi, S.O. Ryu, Optical and electrical properties of transparent conducting gallium-doped ZnO electrodes prepared by atomic layer deposition for application in organic solar cells, Thin Solid Films 546 (2013) 271-274.
- [10] M. Grilli, I. Di Sarcina, S. Bossi, A. Rinaldi, L. Pilloni, A. Piegari, Ultrathin and stable Nickel films as transparent conductive electrodes, Thin Solid Films 594 (2015) 261-265.
- [11] J. Zou, H.-L. Yip, S.K. Hau, A.K.-Y. Jen, Metal grid/conducting polymer hybrid transparent electrode for inverted polymer solar cells, Applied Physics Letters 96(20) (2010).
- [12] Q. Fan, Q. Zhang, W. Zhou, F. Yang, N. Zhang, S. Xiao, X. Gu, Z. Xiao, H. Chen, Y. Wang, Highly conductive and transparent carbon nanotube-based electrodes for ultrathin and stretchable organic solar cells, Chinese Physics B 26(2) (2017) 028801.
- [13] J. Yang, F. Yu, A. Chen, S. Zhao, Y. Zhou, S. Zhang, T. Sun, G. Hu, Synthesis and application of silver and copper nanowires in high transparent solar cells, Advanced Powder Materials 1(4) (2022) 100045.
- [14] M.I. Katsnelson, Graphene: carbon in two dimensions, Materials today 10(1-2) (2007) 20-27.
- [15] J.K. Wassei, R.B. Kaner, Graphene, a promising transparent conductor, Materials today 13(3) (2010) 52-59.
- [16] R. Ishikawa, S. Watanabe, S. Yamazaki, T. Oya, N. Tsuboi, Perovskite/Graphene Solar Cells without a Hole-Transport Layer, ACS Applied Energy Materials 2(1) (2019) 171-175.
- [17] J. Sun, Y. Chen, X. Cai, B. Ma, Z. Chen, M.K. Priydarshi, K. Chen, T. Gao, X. Song, Q. Ji, X. Guo, D. Zou, Y. Zhang, Z. Liu, Direct low-temperature synthesis of graphene on various glasses by plasma-enhanced chemical vapor deposition for versatile, cost-effective electrodes, Nano Research 8(11) (2015) 3496-3504.
- [18] N. Wei, Q. Li, S. Cong, H. Ci, Y. Song, Q. Yang, C. Lu, C. Li, G. Zou, J. Sun, Y. Zhang, Z. Liu, Direct synthesis of flexible graphene glass with macroscopic uniformity enabled by copper-foam-assisted PECVD, Journal of Materials Chemistry A 7(9) (2019) 4813-4822.
- [19] R. Garg, S. Elmas, T. Nann, M.R. Andersson, Deposition methods of graphene as electrode material for organic solar cells, Advanced Energy Materials 7(10) (2017) 1601393.
- [20] V.-D. Tran, S.V.N. Pammi, B.-J. Park, Y. Han, C. Jeon, S.-G. Yoon, Transfer-free graphene electrodes for super-flexible and semi-transparent perovskite solar cells fabricated under ambient air, Nano Energy 65 (2019) 104018.
- [21] M.S.A. Kamel, C.T. Stoppiello, M.V. Jacob, Single-step, catalyst-free, and green synthesis of graphene transparent electrode for organic photovoltaics, Carbon 202 (2023) 150-158.
- [22] I.N. Kholmanov, C.W. Magnuson, A.E. Aliev, H. Li, B. Zhang, J.W. Suk, L.L. Zhang, E. Peng, S.H. Mousavi, A.B. Khanikaev, Improved electrical conductivity of graphene films integrated with metal nanowires, Nano letters 12(11) (2012) 5679-5683.
- [23] T.L. Chen, D.S. Ghosh, V. Mkhitaryan, V. Pruneri, Hybrid Transparent Conductive Film on Flexible Glass Formed by Hot-Pressing Graphene on a Silver Nanowire Mesh, ACS Applied Materials & Interfaces 5(22) (2013) 11756-11761.
- [24] C. Jeong, P. Nair, M. Khan, M. Lundstrom, M.A. Alam, Prospects for Nanowire-Doped Polycrystalline Graphene Films for Ultratransparent, Highly Conductive Electrodes, Nano Letters 11(11) (2011) 5020-5025.
- [25] N. Ye, J. Yan, S. Xie, Y. Kong, T. Liang, H. Chen, M. Xu, Silver nanowire–graphene hybrid transparent conductive electrodes for highly efficient inverted organic solar cells, Nanotechnology 28(30) (2017) 305402.
- [26] S.H. Kim, W.I. Choi, K.H. Kim, D.J. Yang, S. Heo, D.-J. Yun, Nanoscale chemical and electrical stabilities of graphene-covered silver nanowire networks for transparent conducting electrodes, Scientific reports 6(1) (2016) 1-12.

- [27] A.G. Ricciardulli, S. Yang, G.J.A. Wetzelaer, X. Feng, P.W. Blom, Hybrid silver nanowire and graphene-based solution-processed transparent electrode for organic optoelectronics, Advanced Functional Materials 28(14) (2018) 1706010.
- [28] M.S.A. Kamel, A. Al-jumaili, M. Oelgemöller, M.V. Jacob, Inorganic nanoparticles to overcome efficiency inhibitors of organic photovoltaics: An in-depth review, Renewable and Sustainable Energy Reviews 166 (2022) 112661.
- [29] M.S. Kamel, M. Oelgemöller, M.V. Jacob, Sustainable plasma polymer encapsulation materials for organic solar cells, Journal of Materials Chemistry A 10(9) (2022) 4683-4694.
- [30] Y.-X. Zhang, J. Fang, W. Li, Y. Shen, J.-D. Chen, Y. Li, H. Gu, S. Pelivani, M. Zhang, Y. Li, J.-X. Tang, Synergetic Transparent Electrode Architecture for Efficient Non-Fullerene Flexible Organic Solar Cells with >12% Efficiency, ACS Nano 13(4) (2019) 4686-4694.
- [31] M.A. Zafar, O.K. Varghese, F.C. Robles Hernandez, Y. Liu, M.V. Jacob, Single-Step Synthesis of Nitrogen-Doped Graphene Oxide from Aniline at Ambient Conditions, ACS Applied Materials & Interfaces 14(4) (2022) 5797-5806.
- [32] S. Roscher, R. Hoffmann, O. Ambacher, Determination of the graphene–graphite ratio of graphene powder by Raman 2D band symmetry analysis, Analytical Methods 11(9) (2019) 1224-1228.
- [33] M.V. Jacob, R.S. Rawat, B. Ouyang, K. Bazaka, D.S. Kumar, D. Taguchi, M. Iwamoto, R. Neupane, O.K. Varghese, Catalyst-Free Plasma Enhanced Growth of Graphene from Sustainable Sources, Nano Letters 15(9) (2015) 5702-5708.
- [34] H.D. Le, T.T.T. Ngo, D.Q. Le, X.N. Nguyen, N.M. Phan, Synthesis of multi-layer graphene films on copper tape by atmospheric pressure chemical vapor deposition method, Advances in Natural Sciences: Nanoscience and Nanotechnology 4(3) (2013) 035012.
- [35] X. Dong, P. Wang, W. Fang, C.-Y. Su, Y.-H. Chen, L.-J. Li, W. Huang, P. Chen, Growth of large-sized graphene thin-films by liquid precursor-based chemical vapor deposition under atmospheric pressure, Carbon 49(11) (2011) 3672-3678.
- [36] B. Ouyang, Y. Zhang, Z. Zhang, H.J. Fan, R.S. Rawat, Green synthesis of vertical graphene nanosheets and their application in high-performance supercapacitors, RSC Advances 6(28) (2016) 23968-23973.
- [37] A. Al-Jumaili, M.A. Zafar, K. Bazaka, J. Weerasinghe, M.V. Jacob, Bactericidal vertically aligned graphene networks derived from renewable precursor, Carbon Trends 7 (2022) 100157.
- [38] T.R. Gengenbach, G.H. Major, M.R. Linford, C.D. Easton, Practical guides for x-ray photoelectron spectroscopy (XPS): Interpreting the carbon 1s spectrum, Journal of Vacuum Science & Technology A: Vacuum, Surfaces, and Films 39(1) (2021) 013204.
- [39] R. Blume, D. Rosenthal, J.P. Tessonnier, H. Li, A. Knop-Gericke, R. Schlögl, Characterizing graphitic carbon with X-ray photoelectron spectroscopy: a step-by-step approach, ChemCatChem 7(18) (2015) 2871-2881.
- [40] D.J. Morgan, Comments on the XPS Analysis of Carbon Materials, C 7(3) (2021) 51.
- [41] K. Liu, S. Chen, Y. Luo, L. Liu, Hybrid of silver nanowire and pristine-graphene by liquid-phase exfoliation for synergetic effects on electrical conductive composites, RSC advances 4(79) (2014) 41876-41885.
- [42] R. Kaindl, G. Jakopic, R. Resel, J. Pichler, A. Fian, E. Fisslthaler, W. Grogger, B.C. Bayer, R. Fischer, W. Waldhauser, Synthesis of graphene-layer nanosheet coatings by PECVD, Materials Today: Proceedings 2(8) (2015) 4247-4255.
- [43] S. Alancherry, K. Bazaka, I. Levchenko, A. Al-Jumaili, B. Kandel, A. Alex, F.C. Robles Hernandez, O.K. Varghese, M.V. Jacob, Fabrication of nano-onion-structured graphene films from citrus sinensis extract and their wetting and sensing characteristics, ACS applied materials & interfaces 12(26) (2020) 29594-29604.
- [44] H. Li, Y. Liu, A. Su, J. Wang, Y. Duan, Promising hybrid graphene-silver nanowire composite electrode for flexible organic light-emitting diodes, Scientific Reports 9(1) (2019) 1-10.

- [45] B.T. Camic, H.I. Jeong, M.H. Aslan, A. Kosemen, S. Kim, H. Choi, F. Basarir, B.R. Lee, Preparation of transparent conductive electrode via layer-by-layer deposition of silver nanowires and its application in organic photovoltaic device, Nanomaterials 10(1) (2019) 46.
- [46] H. Park, S. Chang, X. Zhou, J. Kong, T.s. Palacios, S. Gradečak, Flexible graphene electrode-based organic photovoltaics with record-high efficiency, Nano Letters 14(9) (2014) 5148-5154.
- [47] H. Hosseinzadeh Khaligh, I.A. Goldthorpe, Hot-rolling nanowire transparent electrodes for surface roughness minimization, Nanoscale Research Letters 9(1) (2014) 1-5.